

## Technology

# Alloys and Composites

### **Magnetic circular dichroism in the x-ray absorption spectra of the CMR compound, $\text{Yb}_{14}\text{MnSb}_{11}$**

Holm, A.P., S.M. Kauzlarich, S.A. Morton, G.D. Waddill, W.E. Pickett, J.G. Tobin

### **Osteoblast-like cell adhesion on bioactive glasses: Surface reactions and resistance to trypsinization**

Foppiano, S., A.P. Tomsia, G.W. Marshall, T. Breunig, D.J. Rowe, S.J. Marshall

### **Photoemission electron microscopy and x-ray magnetic circular dichroism of $\text{Fe}_x\text{Ni}_{(1-x)}$ thin films on Cu(111)**

Sato, Y., T.F. Johnson, S. Chiang, X.D. Zhu, D.P. Land, J.A. Giacomo, F. Nolting, A. Scholl

### **X-ray absorption studies of the cBN composites with different bonding phases**

Benko, E., K. Lawniczak-Jablonska, P. Nachimuthu, I.N. Demchenko, E. Piskorska, P. Klimczyk, R.C.C. Perera, A. Wlochowicz, A. Benko, T.L. Barr

# Magnetic Circular Dichroism in the X-ray Absorption Spectra of the CMR Compound, $\text{Yb}_{14}\text{MnSb}_{11}$

A. P. Holm<sup>1</sup>; S. M. Kauzlarich<sup>1</sup>; S. A. Morton<sup>2</sup>; G. D. Waddill<sup>3</sup>;  
W. E. Pickett<sup>4</sup>; J. G. Tobin<sup>2</sup>

<sup>1</sup>Department of Chemistry, University of California, Davis, CA 95616.

<sup>2</sup>Lawrence Livermore National Laboratory, Livermore, CA 94550.

<sup>3</sup>Department of Physics, University of Missouri-Rolla, Rolla, MO 65401-0249.

<sup>4</sup>Department of Physics, University of California, Davis, CA 95616.

This work is part of ongoing investigations into the magnetic and electronic properties of the rare-earth transition metal Zintl phases  $\text{A}_{14}\text{MnPn}_{11}$  ( $\text{A} = \text{Eu}, \text{Yb}$ ;  $\text{Pn} = \text{Sb}, \text{Bi}$ ) at the Advanced Light Source. We have recently obtained exciting new results from X-ray magnetic circular dichroism (XMCD) investigations of the  $\text{Yb}_{14}\text{MnSb}_{11}$  system. Specifically, we have used XMCD as an element specific probe into the nature of the magnetic moment in this system with the intention of exploring the proposed half-metallic nature of this compound and its related substitutional analogues. Our XMCD measurements indicate that  $\text{Yb}_{14}\text{MnSb}_{11}$  is a half-metallic ferromagnet, and we have submitted our results for publication to Physical Review Letters.

The term half-metallic ferromagnet arises from theoretical predictions made by R.A. de Groot et al based on band structure calculations of the ferromagnetic Heusler alloy  $\text{NiMnSb}$ .<sup>1</sup> These calculations proposed a new phase of matter that displays separate electronic properties for majority-spin and minority-spin electrons. Specifically, one electron spin population is metallic and the other is insulating. Such a material, (possessing 100% spin polarization of the conduction electron) would hold significant technological potential as a single-spin electron source for spintronic devices, data storage applications, and high efficiency magnetic sensors.<sup>2</sup>

The materials we are studying are new compounds that belong to a class of materials called transition-metal Zintl phases. These compounds are isostructural to  $\text{Ca}_{14}\text{AlSb}_{11}$  and crystallize in the tetragonal space group  $I4_1/a$  ( $Z = 8$ ). The  $\text{Yb}_{14}\text{MnSb}_{11}$ ,  $\text{Yb}_{14}\text{MnBi}_{11}$  and  $\text{Eu}_{14}\text{MnSb}_{11}$  analogues are each reported to order ferromagnetically at 56 K, 58 K and 28 K, and 92 K, respectively.<sup>3-6</sup>  $\text{Eu}_{14}\text{MnBi}_{11}$  is an antiferromagnet with a Néel transition at  $T_N = 32$  K.<sup>6</sup> Each of these materials exhibits a large resistance drop associated with their unique magnetic ordering temperature. This behavior is attributed to colossal magnetoresistance effects, and could help support the proposal made by Pickett and Singh of a correlation between half-metallicity and colossal magnetoresistance.<sup>7</sup> These systems are ideal for investigations into the links between magneto-resistance, magnetic moment and half-metallic behavior.

The ability to perform X-ray magnetic circular dichroism experiments on the EPU has allowed us to probe the dichroic characteristics of Mn and Sb in the  $\text{Yb}_{14}\text{MnSb}_{11}$

system during experiments recently performed on beamline 4.0 of the ALS. Figure 1 shows the results from XMCD experiments on the Mn  $L_{23}$ , Sb  $M_{45}$ , and Yb  $N_{45}$  edges of  $\text{Yb}_{14}\text{MnSb}_{11}$ . A dramatic dichroism effect is shown in the Mn  $L_{23}$  region which is confined to one sub-component of the Mn edge and closely matches theoretical models for  $\text{Mn}^{2+}$ ,  $d^5$  dichroism (Figure 1d). The difference in intensity upon change of helicity is greater than 30%, and is strong evidence of a significant moment being present on the Mn. In contrast, no dichroism was observed in the Yb edges, but a small antialigned moment is present in the Sb  $M_{45}$  edges as shown on the left side of Figure 1. This result is surprising because initial models predicted that dichroism would be restricted to the Mn  $L_{23}$  region (with no dichroism in the Sb  $M_{45}$  region) and that it would be  $\text{Mn}^{3+}$ ,  $d^4$  like in character. However, an ongoing collaboration with theoretical groups in the physics departments of the University of California, Davis and the University of Illinois, Urbana to model the Ca and Ba analogues of this structure type has now produced calculated results consistent with our experimental observations of how the Sb behaves in this system. They argue that the Mn should be in a  $2+$ ,  $d^5$  configuration, and the  $\text{Sb}_4$  cage surrounding the Mn should have a hole antialigned to the Mn moment giving a total moment of  $\sim 4 \mu_B/\text{formula unit}$ . Our experimental results are consistent with these new theoretical results, and in addition, these comparisons of data with theoretical calculations and SQUID magnetometry measurements confirm that  $\text{Yb}_{14}\text{MnSb}_{11}$  is indeed a half-metallic ferromagnet.<sup>8-10</sup>

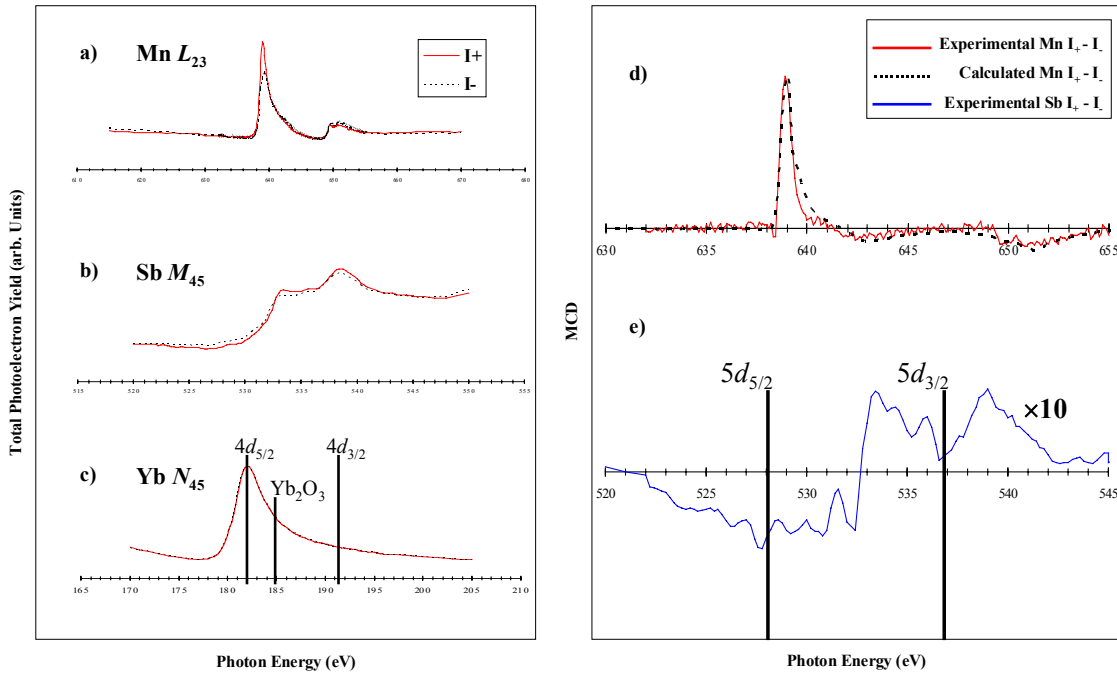


Fig. 1. The raw absorption spectra at plus and minus light polarization for a) Mn  $L_{23}$ , b) Sb  $M_{45}$ , and c) Yb  $N_{45}$  are shown on the left. The XMCD spectra for d) the experimental Mn  $L_{23}$  denoted by a solid red line and the calculated  $\text{Mn}^{2+}$ ,  $d^5$   $L_{23}$  denoted by a dashed black line, and e) the experimental Sb  $M_{45}$  denoted by a solid blue line.<sup>10</sup>

## References:

1. de Groot, R. A.; Mueller, F. M.; van Engen, P. G.; Buschow, K. H. J. *Physical Review Letters* **1983**, *50*, 2024 -2027.
2. Prinz, G. A. *Science* **1998**, *282*, 1660 - 1663.
3. Chan, J. Y.; Kauzlarich, S. M.; Klavins, P.; Shelton, R. N.; Webb, D. J. *Chemistry of Materials* **1997**, *9*, 3132-3135.
4. Chan, J. Y.; Olmstead, M. M.; Kauzlarich, S. M.; Webb, D. J. *Chemistry of Materials* **1997**, *10*, 3583 - 3588.
5. Chan, J. Y.; Wang, M. E.; Rehr, A.; Kauzlarich, S. M.; Webb, D. J. *Chemistry of Materials*. **1997**, *9*, 2131 - 2138.
6. Chan, J. Y.; Kauzlarich, S. M.; Klavins, P.; Shelton, R. N.; Webb, D. J. *Physical Review B* **1998**, *57*, 8103 - 8106.
7. Pickett, W. E.; Singh, D. J. *Physical Review B* **1996**, *53*, 1146 - 1160.
8. Sánchez-Portal, D.; Martin, R. M.; Kauzlarich, S. M.; Pickett, W. E. *Physical Review B* **2001**, *Submitted September 31*.
9. van der Laan, G.; Thole, B. T. *Physical Review B* **1991**, *43*, 13401-13411.
10. Holm, A. P.; Kauzlarich, S. M.; Morton, S. A.; Waddill, G. D.; Pickett, W. E.; Tobin, J. G. *Physical Review Letters* **2001**, *Submitted November 26*.

This work was supported by the Director, Office of Energy Research, Office of Basic Energy Sciences, Materials Science Division, of the U.S. Department of Energy under Contract No. # R5-32633.A02. This work was performed under the auspices of the U.S. Department of Energy by Lawrence Livermore National Laboratory under contract no. W-7405-Eng-48.

Principal Investigator: Susan M. Kauzlarich, Department of Chemistry, University of California Davis, California 95616. Phone: (530)752-4756 fax: (530)752-8995 Email: smkauzlarich@ucdavis.edu

## **Osteoblast-like cell adhesion on bioactive glasses: surface reactions and resistance to trypsinization**

S. Foppiano, A.P. Tomsia<sup>1</sup>, G.W. Marshall, T. Breunig, D.J. Rowe, and S.J. Marshall

(University of California San Francisco and <sup>1</sup>Lawrence Berkeley National Laboratory Berkeley, CA)

A preliminary study was initiated to identify the early stages of apatite formation on bioactive glass substrates. Several bioactive glasses are being examined to determine the effects of glass composition on the early processes of apatite nucleation and growth. The objective of this project is to improve osseointegration of implant materials for dental and orthopedic applications. The high spatial resolution of the FTIR system on beam line 1.4.3 has allowed us to examine small isolated features on the glass surfaces. We are continuing this effort during the next experimental period by examining the progression of apatite formation with increasing exposure time to simulated body fluid.

We have developed bioactive glass coatings of Ti alloys that provide good metal adhesion while retaining bioactivity. Two of the glasses (6P1 and 6P8) proved to be suitable substrates for the attachment of osteoblast-like cells. Osteoblast-like cells, when seeded on glass 6P8, showed remarkable resistance to detachment by trypsinization. The purpose of this study was to investigate two possible mechanisms underlying trypsin resistance of MG63 osteoblast-like cells on glass 6P8: 1) trypsin inactivation by solubility products released from glass 6P8 in tissue culture medium; 2) differential protein adsorption on the substrates. Glass discs of the same dimensions ( $\varnothing = 12$  mm) were finished through 0.05  $\mu\text{m}$  alumina slurry, cleaned by ultra-sonication in alcohol, sterilized in dry heat at 250° C, and placed in 12-well tissue culture plates (N=5 per material). Human osteosarcoma (osteoblast-like) cells (MG63) were cultured in  $\alpha$ -MEM with 10% fetal calf serum and antibiotics.  $4 \times 10^5$  cells in a 20  $\mu\text{L}$  aliquot were plated on each glass or titanium alloy (Ti6Al4V), as a control. Cells were allowed to settle for 1 hr prior to flooding with medium. After 30 min cells were treated with 1.5 mL of trypsin, either fresh or previously incubated for 1 hr with a disc of glass 6P8. Cells were completely detached from Ti6Al4V at 5 min and glass 6P1 at 10 min. After 15 min cells were still adhering onto glass 6P8, as previously observed. Therefore, cell adherence does not seem to be due to glass 6P8 reactivity products inactivating trypsin. Then specimens of the same two glasses and Ti6Al4V (control) (N=4) were prepared, as described above, and incubated with 2 mL of fetal calf serum for 2 hr at 37 °C. Samples were gently rinsed with PBS to remove weakly adsorbed proteins and desorbed with 10 rinses of 500  $\mu\text{L}$  of 0.1% sodium dodecyl sulphate (SDS). The SDS rinses were collected and analyzed for protein concentration, using a spectrophotometric assay (BioRad Laboratories, and Molecular Devices v max kinetic microplate reader) with serum albumin as the standard. Data normalized to sample surface area showed significant differences in the amount of protein adsorbed per unit of surface area among substrates (6P8>6P1>Ti6Al4V, one-way ANOVA  $p<0.001$ ). Aliquots of the same samples were fractionated by SDS-polyacrylamide gel electrophoresis, and the proteins visualized by staining with Coomassie blue. The distribution of the bands indicated differential protein adsorption between the bioactive glasses and Ti6Al4V. Glass surfaces were analyzed by Fourier transform infrared spectroscopy (FTIR) before and after the protein adsorption

experiments to identify surface reactions and residual adsorbed proteins. FTIR surface analysis showed that glass 6P8 readily reacted in solution, forming silanols, while glass 6P1 did not. These results indicate that resistance to trypsinization of osteoblast-like cells from glass 6P8 may be due to differential protein adsorption but not to trypsin inactivation. Supported by NIH/NIDCR Grant DE 11289

Principal investigator: S. Foppiano, University of California, San Francisco, (415) 476-2048

# Photoemission Electron Microscopy and X-Ray Magnetic Circular Dichroism of $\text{Fe}_x\text{Ni}_{(1-x)}$ Thin Films on Cu(111)

Y.Sato<sup>1</sup>, T.F.Johnson<sup>1</sup>, S.Chiang<sup>1</sup>, X.D.Zhu<sup>1</sup>, D.P.Land<sup>2</sup>, J.A.Giacomo<sup>1</sup>  
F.Nolting<sup>3</sup>, and A.Scholl<sup>3</sup>

<sup>1</sup>Dept. of Physics, University of California, Davis, CA 95616

<sup>2</sup>Dept. of Chemistry, University of California, Davis, CA 95616

<sup>3</sup>Advanced Light Source, Lawrence Berkeley National Laboratory, Berkeley, CA 94720

## INTRODUCTION

Our research focuses on controlling the structure, composition and the resultant magnetic properties of metal alloy thin film growth at the atomic level. Better understanding and control of surface/interface magnetism is relevant to the application of the giant magneto-resistive effect to read heads for magnetic recording. We have studied  $\text{Fe}_x\text{Ni}_{(1-x)}$  alloy thin films for their technological relevance to the above mentioned technology. The dependence of the magnetism on the stoichiometry  $x$  is one of the questions of interest. In addressing this problem, the structure of the thin film must be also considered. In terms of crystal structure, a well known “Invar effect” exists in bulk FeNi alloy because of structural incompatibilities of the two elements. Pure Fe is stable in bcc phase whereas pure Ni has fcc structure. A bulk alloy containing more than 65% Fe transforms to bcc by a Martensitic transformation, and the magnetization falls to zero. In thin film alloys, the problem may become more complex because of the effect of substrate structure and interface properties. On the other hand, how this structural change affects the magnetic order in the film is not well known. A simultaneous study of film structure, magnetic structure and magnetism is needed to better understand the system.

Several studies on  $\text{Fe}_x\text{Ni}_{(1-x)}$  alloy thin films have been reported<sup>1,2,3,4</sup>. Information on the growth, structure, and magnetic moments as a function of thickness and concentration has been obtained using various techniques such as low energy electron diffraction (LEED), reflection high energy electron diffraction (RHEED), photoelectron diffraction, surface magneto optical Kerr effect (SMOKE), X-ray magnetic linear dichroism (XMLD), Mossbauer spectroscopy, and superconducting quantum interference device (SQUID) magnetometry. We have used the photoemission electron microscope (PEEM2) at the Advanced Light Source (beamline 7.3.1.1) to study this film system. PEEM has the unique capability of imaging the film’s magnetic structure with high spatial resolution and elemental specificity. Simultaneously, quantitative magnetic information can be obtained using magnetic circular dichroism in X-ray absorption spectroscopy. At two different thicknesses, we have made sixteen samples and studied the dependence of magnetic structure on varying Fe concentration and substrate quality ( $x = 0, 0.28, 0.55, 0.6, 0.66, 0.74, 1.0$  at  $10\text{\AA} \approx 5\text{ML}$ ,  $x = 0.9, 0.25, 0.33, 0.42, 0.5, 0.55, 1.0$  at  $20\text{\AA} \approx 10\text{ML}$ ). We have observed clear ferromagnetic domain structures of the film on a Cu(111) surface for  $x \leq 0.60$  at room temperature.

## RESULTS

Samples with high Fe content ( $x=0.66, 0.74$  at 5ML) have been observed to be non-magnetic at room temperature. All other alloy samples ( $x \leq 0.6$ , 5ML and 10ML) showed clear ferromagnetic contrast. This trend of reduction in Curie temperature at higher Fe concentration is also observed by spin resolved photoemission spectroscopy measurements carried out at the Advanced Light Source (beamline 7.0.1.2). A pure Ni film at 5ML thickness was non-magnetic at room temperature. According to a SMOKE measurement, 5ML is approximately the thickness where the Curie temperature becomes less than room temperature for Ni/Cu(111)<sup>5</sup>.

Fig. 1 shows typical ferromagnetic images with a  $12\mu\text{m}$  field of view for a 5ML thick  $\text{Fe}_{0.6}\text{Ni}_{0.4}$  film on Cu(111). Each image is obtained by dividing an image acquired at the L3 Fe (or Ni) edge by one acquired at the L2 Fe (or Ni) edge. The images show alignment of the magnetic domains for

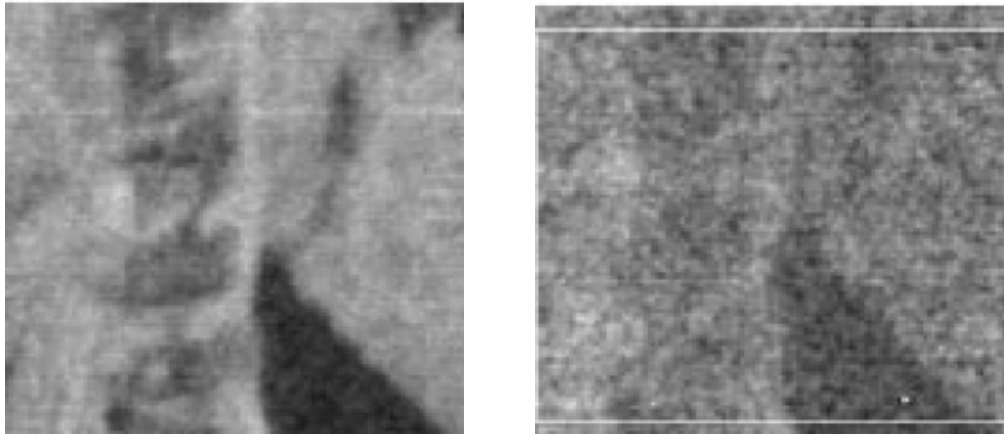


Fig. 1. XMCD ferromagnetic images with a  $12\mu\text{m}$  field of view for a 5ML thick  $\text{Fe}_{0.6}\text{Ni}_{0.4}/\text{Cu}(111)$ . Left: Fe XMCD contrast, Right: Ni XMCD contrast.

Fe and Ni, suggesting that Fe and Ni form a good alloy on this surface. By comparing the images shown in Fig. 2 and Fig. 3, we find a clear dependence of the domain structures on film thickness and substrate quality. Fig. 2 shows magnetic contrast images of 5ML alloy films on a mechanically polished substrate. On these samples, observed magnetic structures appear to correlate to surface topographic features. No regular appearance of domain structure was seen. Comparison of the image at the pre-absorption edge, which shows only topographic contrast, with the magnetic contrast image clearly shows the correlation between surface structural features and the formation of magnetic domains. An experiment showed that magnetic contrast observed at room temperature disappears gradually upon heating. Contrast is recovered again as the sample temperature is lowered below the Curie temperature. This also confirms the relation between domain structure and surface geometric structures. These observations are consistent for each 5ML sample analyzed. In contrast, for 10ML films on an electropolished substrate as shown in Fig. 3, pinning due to surface defects is observed less frequently. Magnetic structures and textures appear to be more uniform and the sizes of the structures were smaller and on the order of  $1\text{-}3\mu\text{m}$ . At the alloy composition of  $x=0.44$ , regular, periodic appearance of larger domain structures ( $5\text{-}10\mu\text{m}$  width and  $70\mu\text{m}$  length), defined by  $180^\circ$  domain walls, are observed, as shown in Fig. 4. By observing the two images shown in Fig. 4, we conclude that alloy film at this composition and thickness show in-plane magnetization.

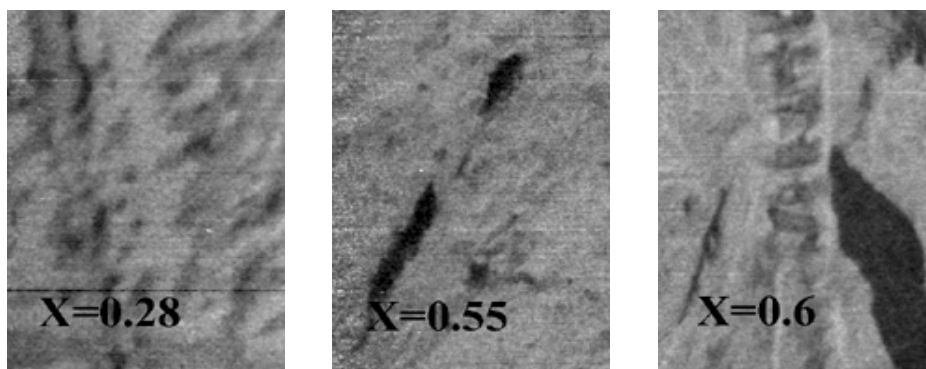


Fig. 2. XMCD ferromagnetic images with  $H22\mu\text{m} \times V30\mu\text{m}$  field of view for 5ML films with varying Fe composition  $x$ .

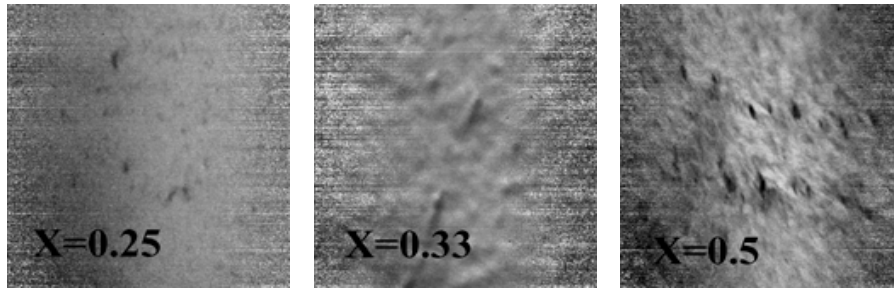


Fig. 3. XMCD ferromagnetic images with  $65\mu\text{m} \times 65\mu\text{m}$  field of view for 10ML films with varying Fe composition  $x$ .

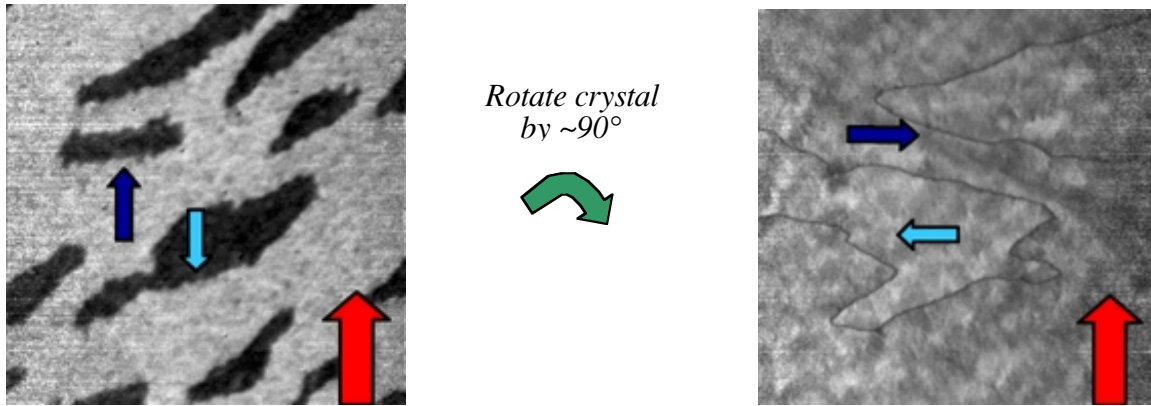


Fig. 4. XMCD ferromagnetic images with Right:  $45\mu\text{m} \times 45\mu\text{m}$  and Left:  $45\mu\text{m} \times 45\mu\text{m}$  field of view for 10ML thick  $\text{Fe}_{0.56}\text{Ni}_{0.44}/\text{Cu}(111)$ . Smaller arrows indicate the magnetization direction and larger arrows show the direction of the incident photon momentum.

## REFERENCES

1. F.O.Schumann, S.Z.Wu, G.J.Mankey, and R.F.Willis *Phys. Rev. B* **56** 2668 (1997)
2. F.O.Schumann, R.F.Willis, K.G.Goodman, and J.G.Tobin *Phys. Rev. Lett.* **79** 5166 (1997)
3. J.W.Freeland, I.L.Grigorov, and J.C.Walker *Phys. Rev. B.* **57** 80 (1998)
4. R.Schellenberg, H.Meinert, N.Takahashi, F.U.Hillebrecht, and E.Kisker *J. App. Phys.* **85** 6214 (1999)
5. R.Zhang, and R.F.Willis *Phys. Rev. Lett.* **86** 2665 (2001)

This work was supported by the Campus Laboratory Collaboration Program of the University of California Office of the President and by the Director, Office of Energy Research, Office of Basic Energy Sciences, of the U.S. Department of Energy under Contract No. DE-AC03-76SF00098.

Principal investigator: Shirley Chiang, Department of Physics, University of California, Davis, CA 95616-8677.  
Email: [chiang@physics.ucdavis.edu](mailto:chiang@physics.ucdavis.edu). Telephone: 530-752-8538.

# X-RAY ABSORPTION STUDIES OF THE cBN COMPOSITES WITH DIFFERENT BONDING PHASES

E. Benko<sup>a</sup>, K. Lawniczak-Jablonska<sup>b</sup>, P. Nachimuthu<sup>c</sup>, I. N. Demchenko<sup>b</sup>, E. Piskorska<sup>b</sup>, P. Klimczyk<sup>a</sup>,  
R.C.C Perera<sup>c</sup>, A. Włochowicz<sup>d</sup>, A. Benko<sup>e</sup>, T. L. Barr<sup>e</sup>

<sup>a</sup>*Institute of Metal Cutting, Wroclawska 37A Str., 30-011 Cracow, Poland*

<sup>b</sup>*Institute of Physics Polish Academy of Science, Al. Lotnikow 32/46, 02-668 Warsaw, Poland*

<sup>c</sup>*Center for X-ray Optics, Lawrence Berkeley National Laboratory, University of California –Berkeley, Berkeley, California 94720*

<sup>d</sup>*University of Bielsko Biala , Willowa 2 Str., 43-309 Bielsko-Biala*

<sup>e</sup>*Materials Department and Laboratory for Surface Studies, University of Wisconsin-Milwaukee, Milwaukee, WI 53201, USA*

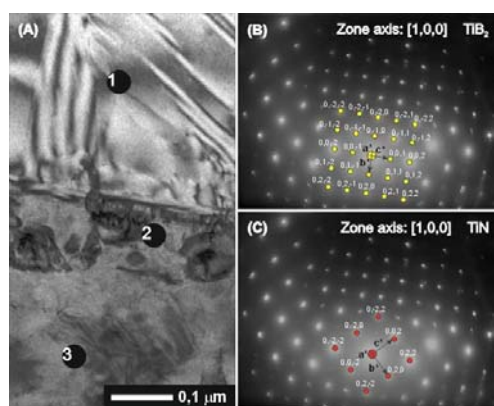
The cBN composites are widely used in various applications because of their excellent wear and corrosion resistance and their thermal and electronic properties. In order to obtain composition materials with optimal properties and using economic and safe for environment technology it is important to recognize chemical reactions occurring at boron nitride during formation of bonding phase. Titanium and their compounds are most commonly used as binders in sintering technology. We present the results of studies of cBN composites with addition of TiN and TiC ceramics to form a bonding phase. The wider class of additions is under investigation.

From thermodynamical calculations it follows that in the temperature range from 1000 to 1400°C TiC and TiN react with cBN forming in the case of TiC two new phases (TiB<sub>2</sub> and TiC<sub>0.8</sub>N<sub>0.2</sub>) and only TiB<sub>2</sub> phase in the case TiN addition.

Composites were prepared by high pressure (9GPa) hot pressing (1750°C) and the samples were subsequently heat treated at 1000 and 1400°C for 1 hour in vacuum 3\*10<sup>-3</sup> Pa. Sinters of cBN-TiN/TiC before and after heat treatment were characterised using transmission electron microscopy and X-ray absorption technique.

## RESULTS AND DISCUSSION

### *TEM studies of the microstructure in cBN sintered with TiN and heated up to 1400°C*



The microstructure of cBN sintered with TiN is compact. Analysis of the electron diffraction (Fig.1, B and C) allowed to conclude that the fine crystallites at the boundary show the TiB<sub>2</sub> phase (B) whereas the bigger grains inside the TiN phase (C). The cBN/TiC compact looks the same like cBN/TiN. But in some places the electron diffraction pattern indicates on the presence of the triple Ti(BC) compound.

Fig.1. Boundary between the two fine-crystalline area of cBN/TiN composite (A) and electron diffraction pattern from the point 2 (B) and 3 (C).

### *X-ray absorption study*

X-ray absorption measurements were carried out at the Advanced Light Source of Lawrence Berkeley National Laboratory (beamline 6.3.2) and at the HASYLAB in Hamburg. (beamline A1). As an example are presented XANES at the Ti K-edge of cBN/TiN (Fig.2) and

Ti  $L_{2,3}$ -edge ( Fig.3) from cBN - TiC/TiN.

Spectra show formation of the  $TiB_2$  new phase after heating to  $1300^{\circ}C$ , without heat treatment  $TiB_2$  was not formed (Fig.2). The formed  $TiB_2$  phase is not ideal, it can have defects and inclusions of other phases. The possibility of the foreign phases addition was check (upper curves) and conclusion can be drawn that addition to the  $TiB_2$  phase up to 30% of TiN phase does not improve the agreement between modelled and observed phase. In composites without heat treatment the inclusions of up to 20% TiC and 10%  $TiB_2$  cannot be excluded.

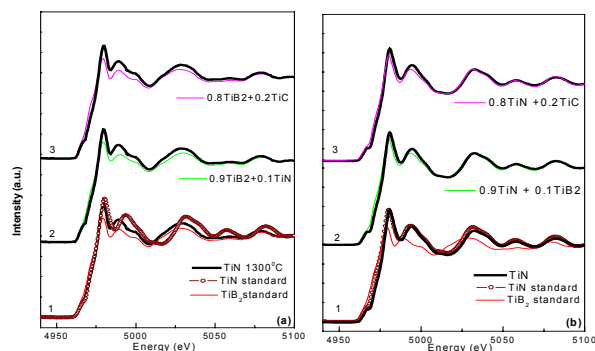


Fig. 2. The Ti K - edges of the cBN/TiN and reference samples heated up to  $1300^{\circ}C$  (a) and cBN/TiN without heat treatment (b).

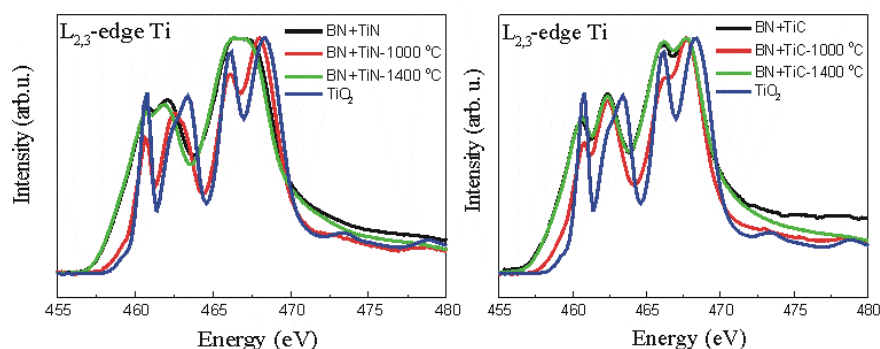


Fig.3. Ti  $L_{2,3}$  x-ray absorption edge spectra of cBN/TiN and cBN/TiC composites before and after heat treatment and  $TiO_2$  as reference.

The pick structure in Fig.3 shows formation of  $TiO_2$  like phase in the cBN-TiN/TiC composites. It was proved that the temperature of  $1000^{\circ}C$  was not high enough to avoid the oxidation of the composite grains, the heat treatment up to  $1400^{\circ}C$  prevent the oxidation of grains.

## Conclusion

X ray absorption measurements provide a clear spectroscopic signature of  $TiB_2$  formation in the cBN-TiN/TiC composites. There was proved that the temperature of  $1000^{\circ}C$  was not high enough to avoid the oxidation of the composite grains, therefore the heat treatment is necessary. The formed  $TiB_2$  phase is not free from the defects but we do not observed foreign phase inclusion after heating.

From the analysis of the edge shape one can conclude on the chemical processes and optimise of the BN-TiC/TiN composites heat treatment procedure.

## Acknowledgements

This study is based on the work sponsored by Polish State Committee for Scientific Research (Grant No 7T08D 014 17) and SPUB (Grant No-M/DESY/P-03/ DZ-213/2000) and IHP-Contract HPRI-CT-1999-00040 of the European Commission.

Principal investigator: Krystyna Lawniczak-Jablonska, Institute of Physics, Polish Academy of Sciences. Telephone: 48 22 8436034. Email: jablo@ifpan.edu.pl.